Electronic Supplementary Material (ESI) for Journal of Materials Chemistry A.

Supporting information

Scalable Preparation of CuO Nanosheet Array via Corrosion Engineering for Selective C-C Coupling in CO_2 Electroreduction

Mang Wang, Lili Wan, Jinshui Cheng and Jingshan Luo*

Institute of Photoelectronic Thin Film Devices and Technology, Solar Energy Research Center, Key Laboratory of Photoelectronic Thin Film Devices and Technology of Tianjin, Ministry of Education Engineering Research Center of Thin Film Photoelectronic Technology, Renewable Energy Conversion and Storage Center, Nankai University, Tianjin 300350, China

*Email: jingshan.luo@nankai.edu.cn (J. Luo)

Supplementary Methods

Chemicals and materials

The Cu mesh (100 mesh, 99.99%) and Nickel foam (NF, 99.9%) was purchased from Suzhou jiashide metal foam Co., Ltd. The NaOH, KOH and $KHCO_3$ (99.99%) were purchased from Aladdin. The H_2SO_4, ethanol and acetone were analytical pure and purchased from SHIJIKEBO Co. Ltd. The Cu pellets (99.999%) were purchased form ZhongNuo Advanced Material (Beijing) Technology Co. Ltd. The ultrapure water (DI water) was used in all the experiments (Sartorius-mini plus UV, 18.2 MΩ·cm).

Preparation of Cu@CuO NS-x electrodes

The Cu@CuO NS-x electrodes were prepared via the spontaneous corrosion of Cu in an alkaline solution, where the Cu mesh was used as substrate and pretreated by acetone, ethanol, diluted H_2SO_4 and DI water. Then, the pretreated Cu mesh was immersed horizontally in a solution of 0.1 M NaOH of 500 mL in a capped plastic box under room temperature, and different electrodes could be prepared after desired corrosion time. Finally, these electrodes were rinsed with DI water repeatedly before dried in a vacuum oven at 60 ˚C overnight.

Preparation of Cu and CuO NS GDE

The Cu GDE was prepared using thermal evaporation (POLDI intelligent Equipment CO., LTD). Briefly, Cu of 300 nm was evaporated onto the GDL (Sigracet 22 BB) under the pressure of $4*10^{-4}$ Pa with an evaporation rate of 0.2 nm s^{-1}.

The CuO NS GDE was prepared following the similar protocol as the Cu@CuO NS electrode, where 0.1 M NaOH of 500 mL was used as the corrosion solution. The Cu GDE was placed on the surface of the solution up-side down. Finally, the CuO NS GDE was rinsed carefully after 12 h reaction and dried in a vacuum oven at 60 ˚C overnight.

Material characterization

The X-ray diffraction (XRD) patterns were obtained with a Rigaku SmartLab 9.0 using Cu Kα radiation (λ = 1.54056 Å), and the data were collected in Bragg-Brettano mode in the 2θ range from 10° to 80° at a scan rate of 5° min^{-1}. The scanning electron microscopy (SEM) images were captured on a JSM-7800F field-emission scanning electron microscope operated at an acceleration voltage of 15 kV. The transmission electron microscopy (TEM) images were collected on a FEI Tecnai G2 F30 S-TWIN transmission electron microscope with an acceleration voltage of 300 kV. The X-ray photoelectron spectroscopy (XPS) spectra were taken on a ThermoFisher ESCALAB™ 250Xi surface analysis system using a monochromatized Al Kα small-spot source, and the corresponding BEs were calibrated by referencing the C 1s to 284.8 eV.

Electrochemical CO_2 (ECO_2 RR) reduction measurements

ECO_2 RR measurement in an H-type cell was carried in a gastight two-compartment electrochemical cell with a three-electrode configuration. Typically, the Cu@CuO NS-x was used as working electrode (WE) and mounted in the cathodic compartment with an active area of 0.5×0.5 cm^2, and a Ag/AgCl reference electrode (RE, Saturated KCl, Tjaida) was used to monitor the potential on the WE. A Ti@IrO_2 electrode with an active area of 1 cm^2 was used as the counter electrode (CE) and mounted in the anodic compartment.[1] A piece of anion-exchange membrane (Selemion AMVN, AGC Inc.) was used to separate the cathodic and anodic compartments to eliminate the crossover and oxidation of the liquid products at the anode surface. The volumes of catholyte and anolyte were 8 mL and 8 mL, respectively. The headspace of the cathodic compartment was about 6 mL. The CO_2-saturated 0.1 M $KHCO_3$ aqueous solution (pH 6.8) was used as the electrolyte and CO_2 gas was introduced into catholyte at a flow rate of 10 standard cubic centimeters per minute (SCCM) controlled by a mass flow controller (MFC) during the electrocatalytic reaction. The electrolyte was stirred by a stir bar during the electrolysis. The cell was connected to a potentiostat (Autolab) and chronoamperometry mode (CA) were performed for 40 minutes at different potentials for performance tests. The performance of all the electrodes at each potential was repeated for at least three times. The potential (E) was converted to the reversible hydrogen electrode (RHE) scale with 90% iR correction using the following equation, where R is the solution resistance between the WE and RE.

$$E\ (vs.\ \mathrm{RHE}) = E\ (vs.\ \mathrm{Ag/AgCl}) + 0.1976 + 0.059*\mathrm{pH} + 90\%*iR$$

The ECO_2 RR measurement in a flow cell was carried out in a three-compartment electrochemical cell with a three-electrode configuration. The Cu or CuO NS GDE with active area of 1 cm^2 was sandwiched between CO_2 gas chamber and catholyte chamber, with the catalyst layer interfaced with the electrolyte. An Ag/AgCl electrode mounted near the GDE was used as the reference electrode. A piece of NF mounted in the anolyte compartment was adopted as the anode for water oxidation reaction. A piece of AEM was placed between the catholyte and anolyte to separate the two chambers. During the experiment, CO_2 was introduced into the CO_2 gas chamber at a constant rate of 20 SCCM controlled by a MFC. Aqueous solution of 1 M KOH or 1 M $KHCO_3$ of 10 mL were circulated through the electrolyte compartment with a flow rate of 10 mL min^{-1}. Chronoamperometric mode (CP) was applied for 40 minutes under each current density. The performance of all the electrodes at each current density was repeated for at least three times, and the FE for gas products was carefully calculated based on the outlet gas flow rate measured by a flowmeter (ADM G6691A). The potential (E) was converted to a pH-independent reference (NHE) due to the change of pH of catholyte during the electrolysis using the following equation.

$$E\ (vs.\ \mathrm{NHE}) = E\ (vs.\ \mathrm{Ag/AgCl}) + 0.1976$$

Electrochemical CO (ECO RR) reduction measurements

The configuration of the flow cell used in ECO RR was the same as the CO_2 RR configuration described above except that CO gas was infused to the gas chamber at a constant rate of 20 SCCM, and the FE for gas products was carefully calculated based on the outlet gas flow rate measured by a flowmeter (ADM G6691A).

Product analysis

The gaseous products were detected by an on-line gas chromatograph (GC, Thermo Fisher) equipped with a thermal conductivity detector (TCD) for hydrogen (H_2) and two flame ionization detectors (FID) for CO, methane (CH_4), ethane (C_2H_6) and ethylene (C_2H_4). The peak identification and peak area were calibrated using standard calibration gas with known concentrations of H_2, CO, CH_4, C_2H_6 and C_2H_4 mixed with CO_2 from a commercial supplier (Dalian GuangMing Special Gas Products Co. Ltd.). The liquid products were quantified with high performance liquid chromatograph (HPLC, Agilent 1260 Infinity). The formate (HCOONa) and acetate (CH_3COONa) were detected using variable wavelength detector (VWD, 210 nm), and ethanol, acetone, n-propanol and acetaldehyde were detected by refractive index detector (RID). The peak area was calibrated using standard solutions prepared with known concentrations of sodium formate, sodium acetate, ethanol, acetone, n-propanol and acetaldehyde. After electrolysis, 900 μL of the catholyte and anolyte were acidized with 100 μL of 4.5 M H_2SO_4 respectively, and the FE for liquids was calculated by adding up both anodic and cathodic FEs.

Double-layer capacitances measurement

The electrochemical double layer capacitance (C_{dl}) was measured by running the electrodes in a non-Faradaic region at 20, 40, 60, 80, 100, 120, 160 mV/s scan rate and fitting the charging current linearly. The electrodes were pre-reduced at -1.0 V *vs*. RHE for 5 minutes before measurement.

CO stripping experiment

The CO stripping experiments were performed in aqueous solution of 0.5 M $LiClO_4$ (pH=6.5) in an H-type cell under CO or N_2 purging. The Cu mesh and Cu@Cu NS were used as the working electrodes respectively. The Ag/AgCl and Ti@IrO_2 were used as the RE and CE respectively. The electrolyte was bubbled for at least 20 minutes prior to all experiments to allow for CO or N_2 saturation. A scan rate of 10 mV/s was used for all experiments.

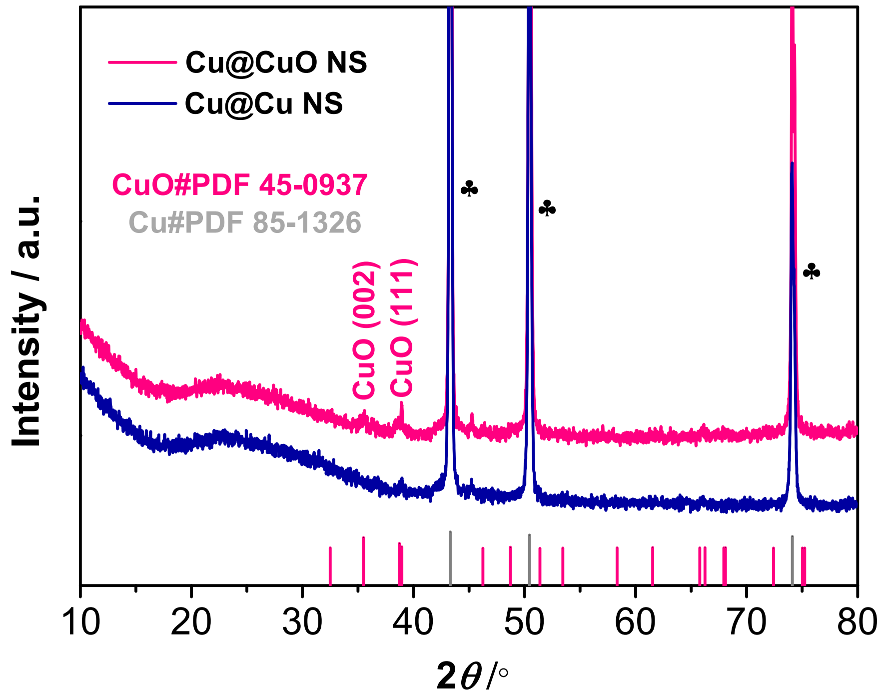

Figure S1. XRD patterns of the Cu@CuO NS-12 and Cu@Cu NS-12 electrodes.

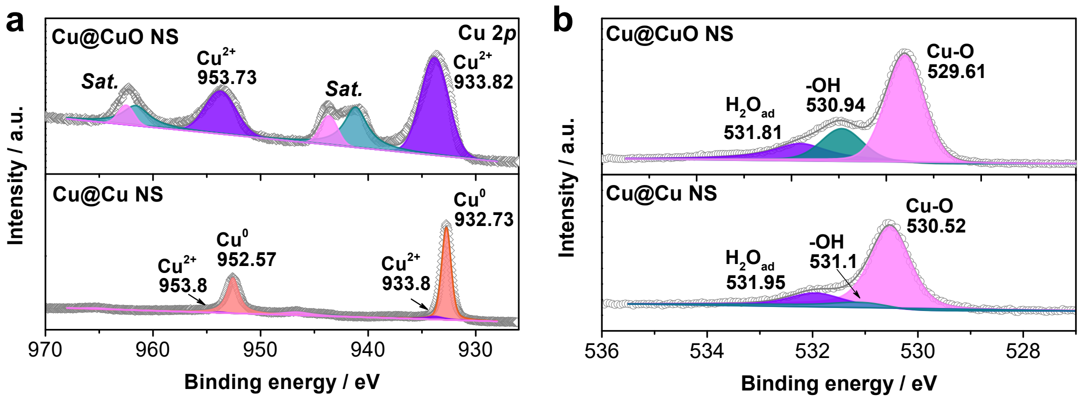

Figure S2. (a) Cu *2p* XPS spectra and (b) O *1s* spectra of the Cu@CuO NS-12 and Cu@Cu NS-12 electrodes.

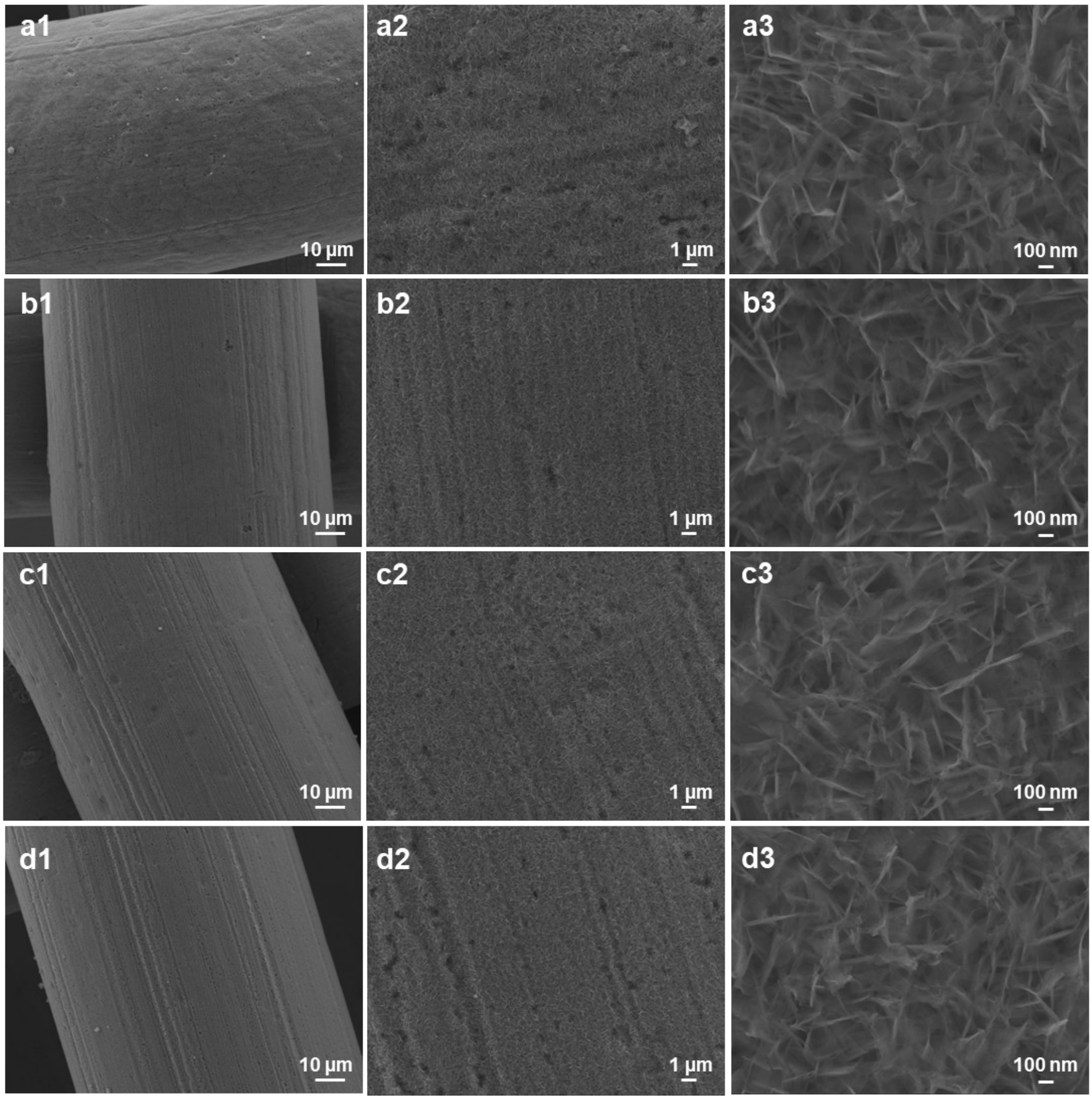

Figure S3. SEM images taken from four different areas of Cu@CuO NS-12 electrode, demonstrating the uniformity of the electrode and the success of the corrosion engineering.

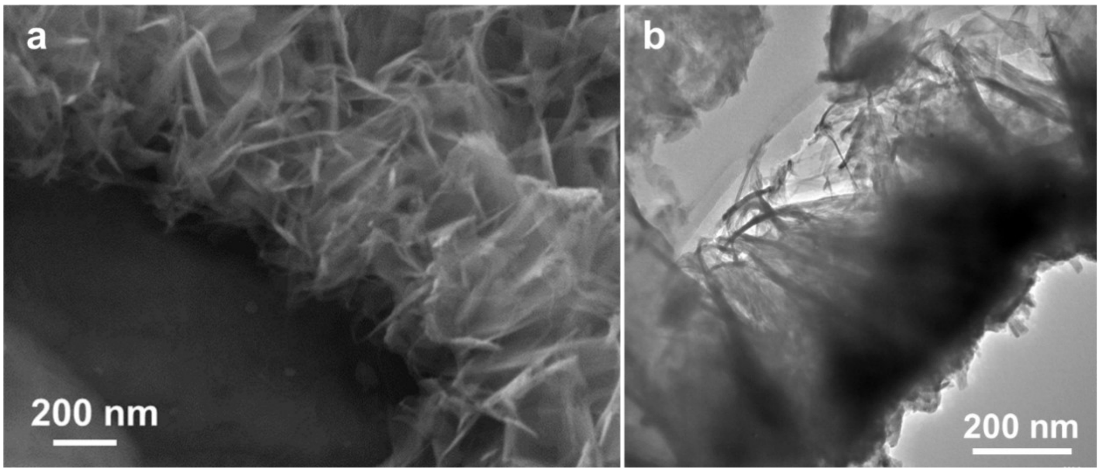

Figure S4. (a) SEM image of a scratch on the Cu@CuO NS-12 electrode, (b) TEM image of a piece of CuO NS array, both of them demonstrate the height of about 300 nm of the CuO NS array.

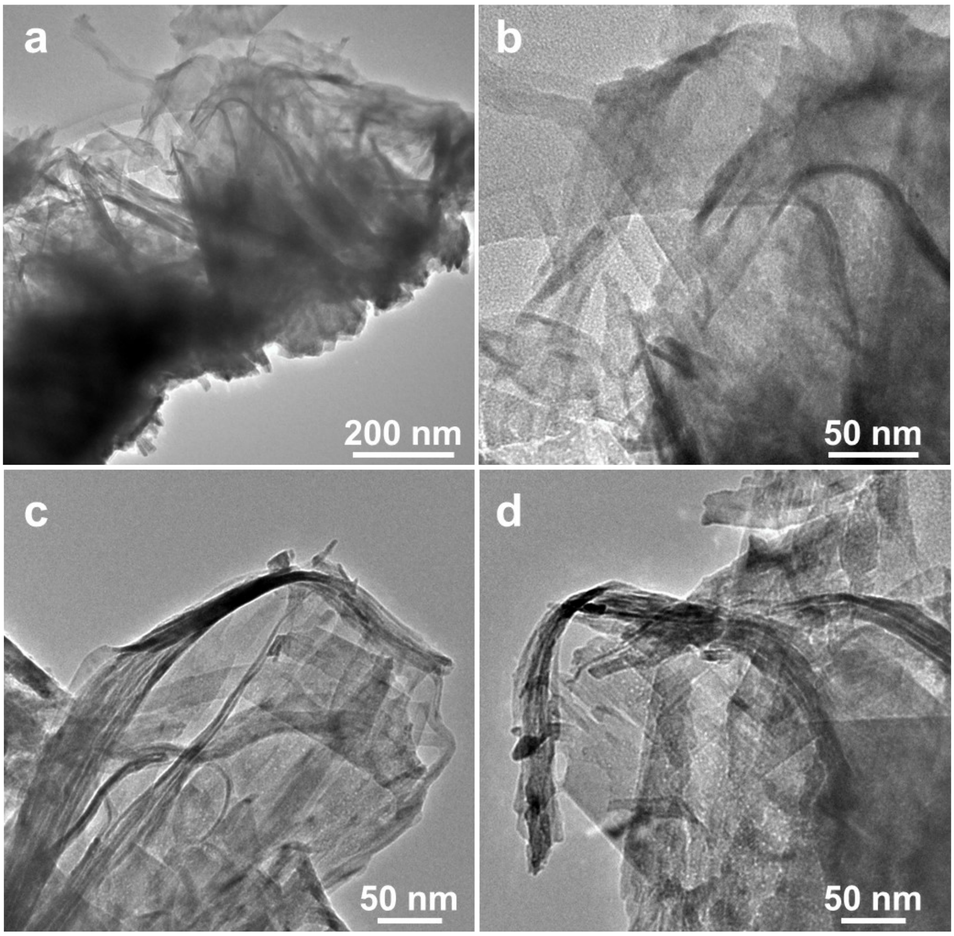

Figure S5. TEM images of the CuO NS detached from the Cu@CuO NS-12 electrode.

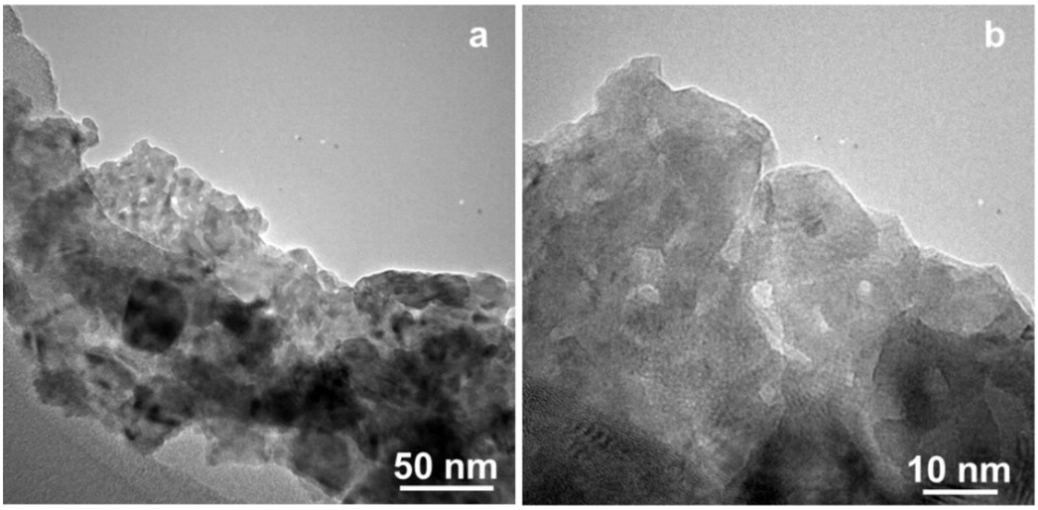

Figure S6. TEM images of the Cu nanosheets with abundant nanopores on the surface.

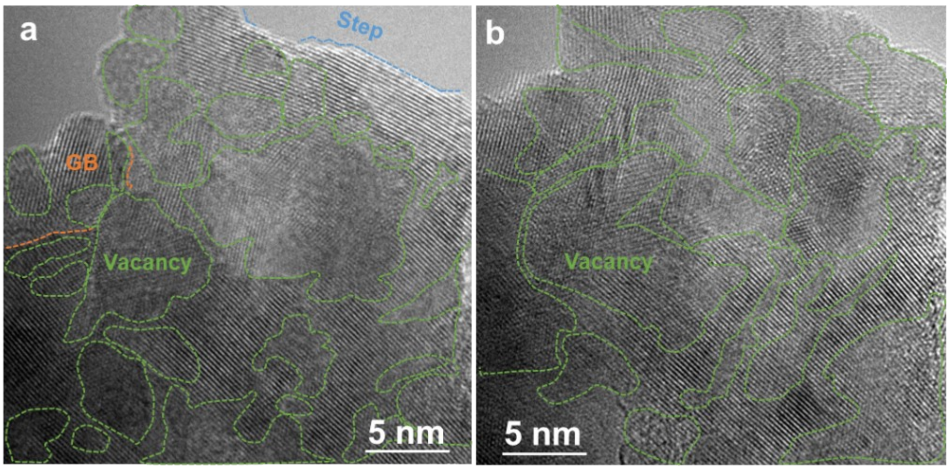

Figure S7. TEM images of two Cu nanosheets show abundant defects (including vacancies, GB and step) on the surface.

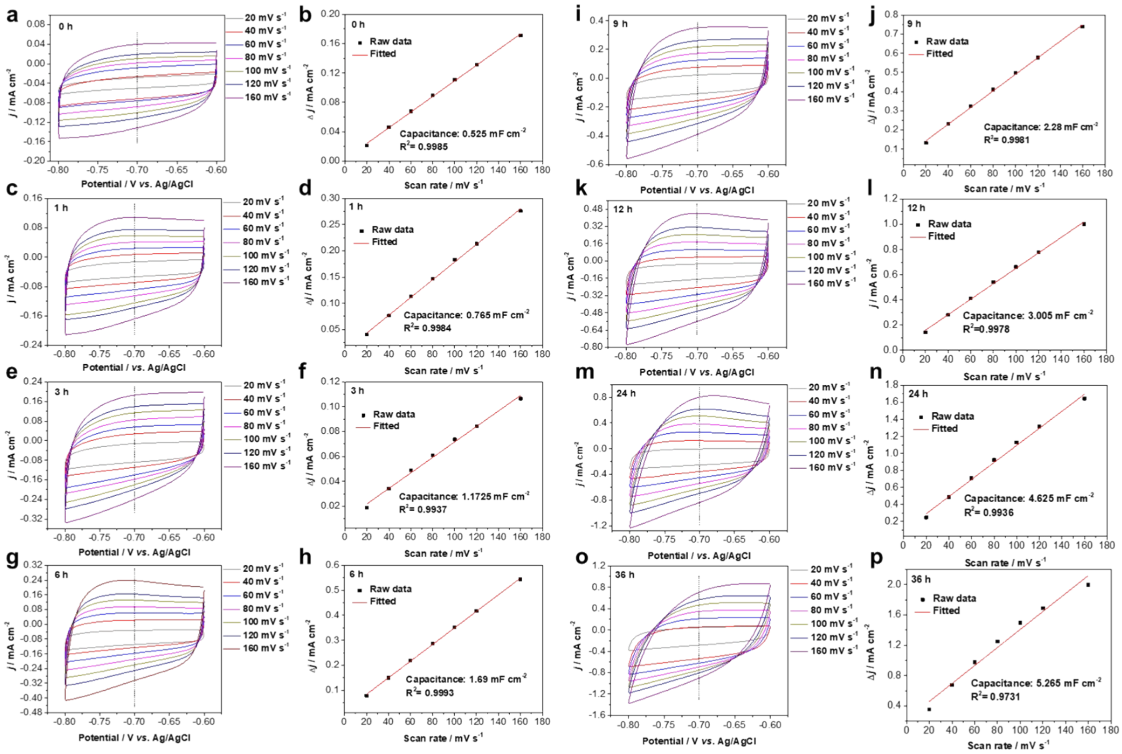

Figure S8. CV curves and the corresponding plots of the capacitive current density at -0.7 V *vs*. Ag/AgCl with respect to the scan rate for Cu mesh at different corrosion stages, (a, b) for 0 h; (c, d) for 1 h; (e, f) for 3 h; (g, h) for 6 h; (I, j) for 9 h; (k, l) for 12 h; (m, n) for 24 h; (o, p) for 36 h.

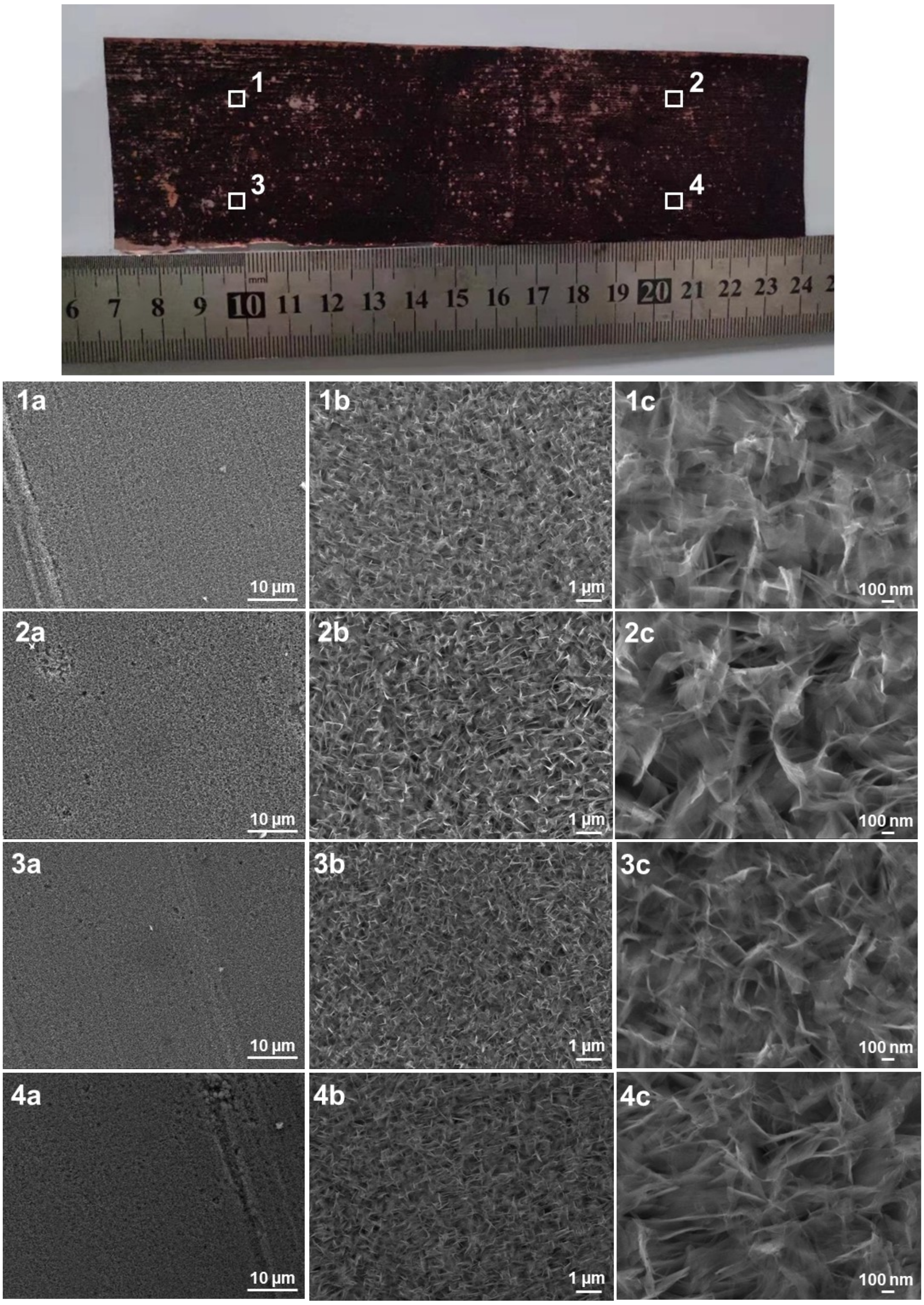

Figure S9. Picture of a large Cu foil@CuO NS electrode with an area of 17×4 cm^2; and the corresponding SEM images at the marked areas 1-4, respectively.

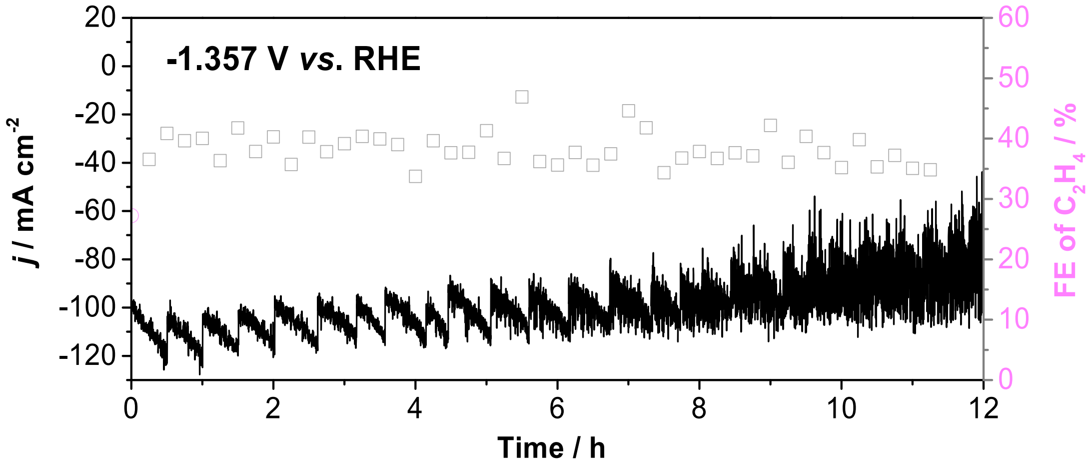

Figure S10. Chronoamperometric curve and the FE of C_2H_4 on the Cu@Cu NS-12 over the course of 12 h electrolysis at -1.357 V *vs*. RHE in 0.1 M $KHCO_3$. The electrolyte was stirred with two magnetic bars under a speed about 1000 rpm. The gradually enlarged fluctuation of current density in the last 4 hours might be due to the rapid water consumption under a high current density and the vaporization of the water.

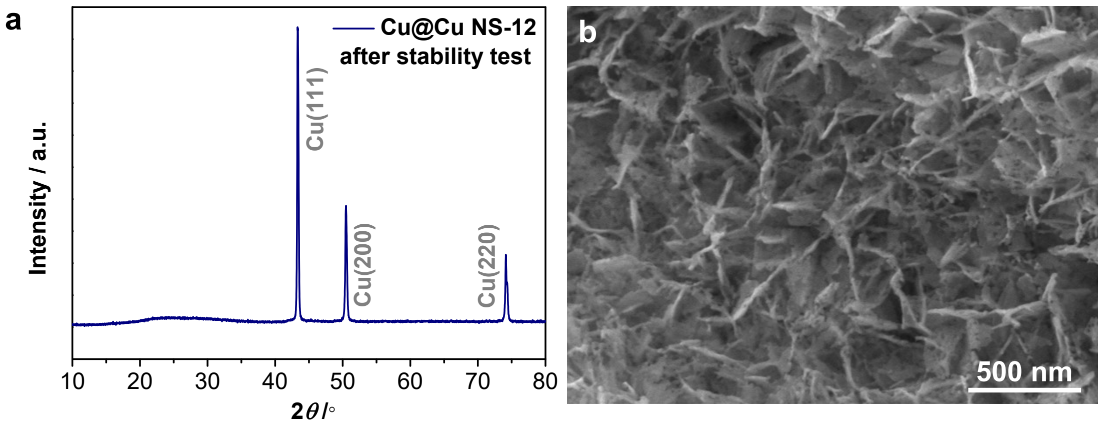

Figure S11. (a) XRD pattern and (b) SEM image of the Cu@Cu NS-12 electrode after stability test.

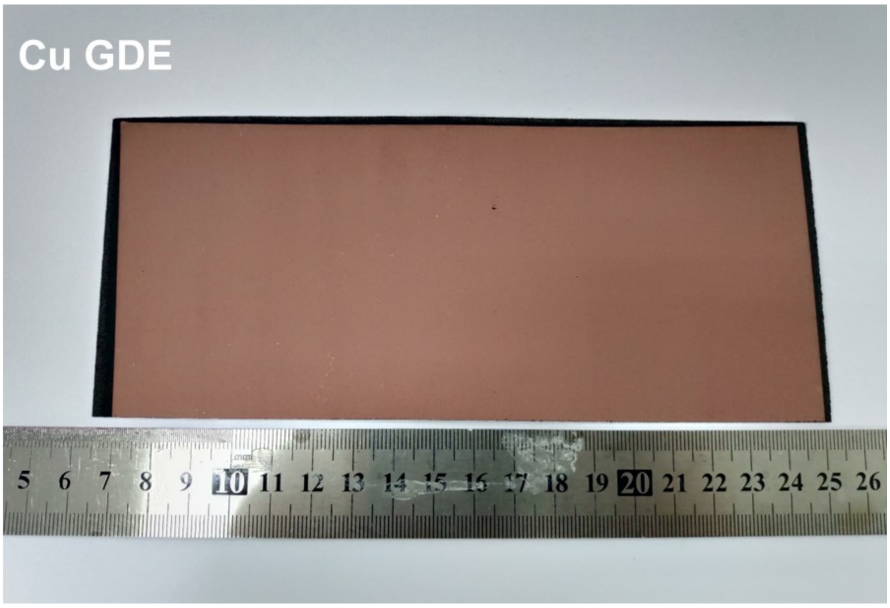

Figure S12. Picture of the pristine Cu GDE with an area of 18×8.5 cm^2.

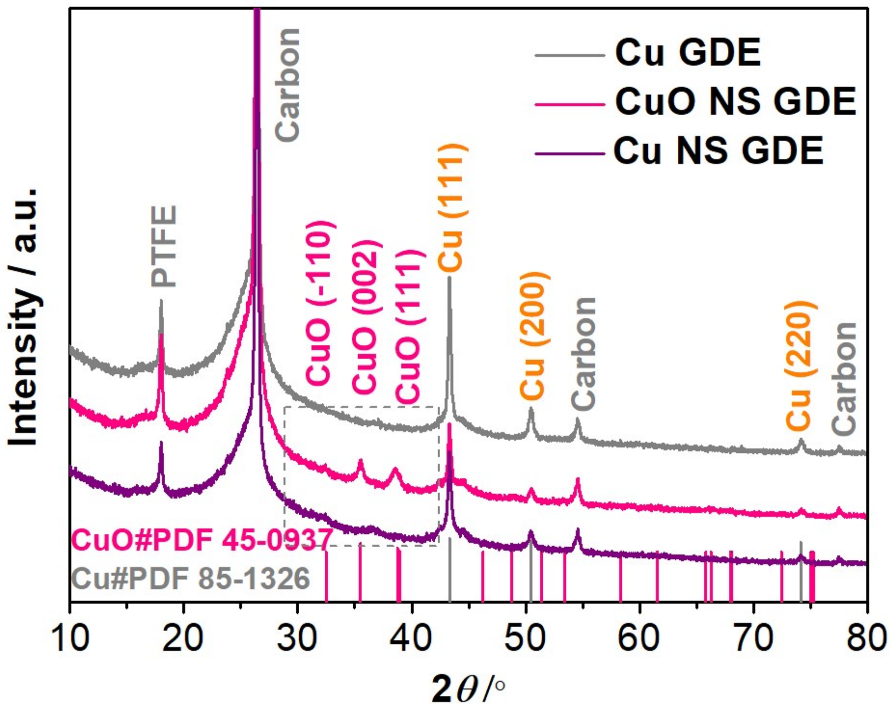

Figure S13. XRD patterns of the pristine Cu GDE (grey line), CuO NS GDE (pink line), and the Cu NS GDE (violet line).

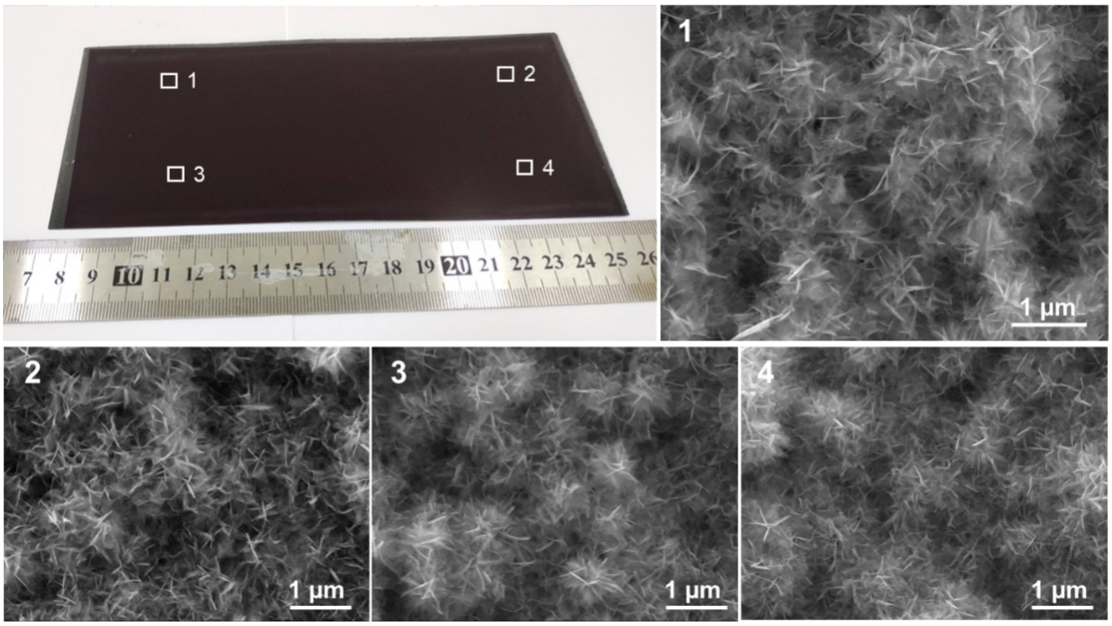

Figure S14. Picture of the CuO GDE with an area of 18×8.5 cm^2, and the corresponding SEM images at the marked areas of 1-4, respectively.

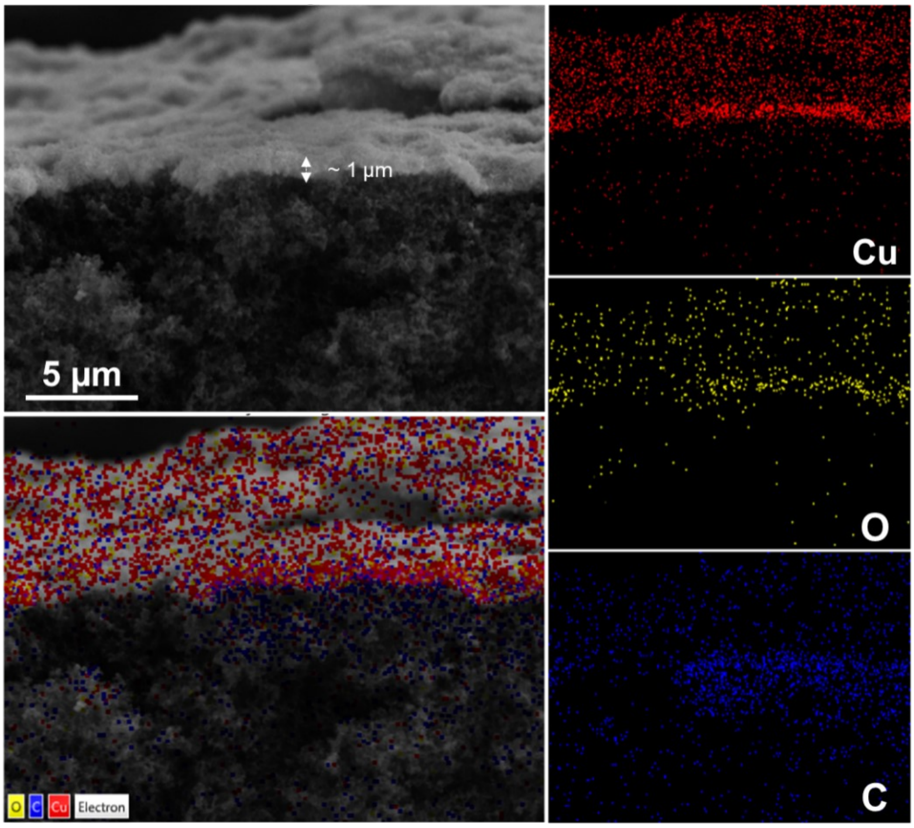

Figure S15. Cross section SEM and the EDS elemental mapping of the CuO NS GDE.

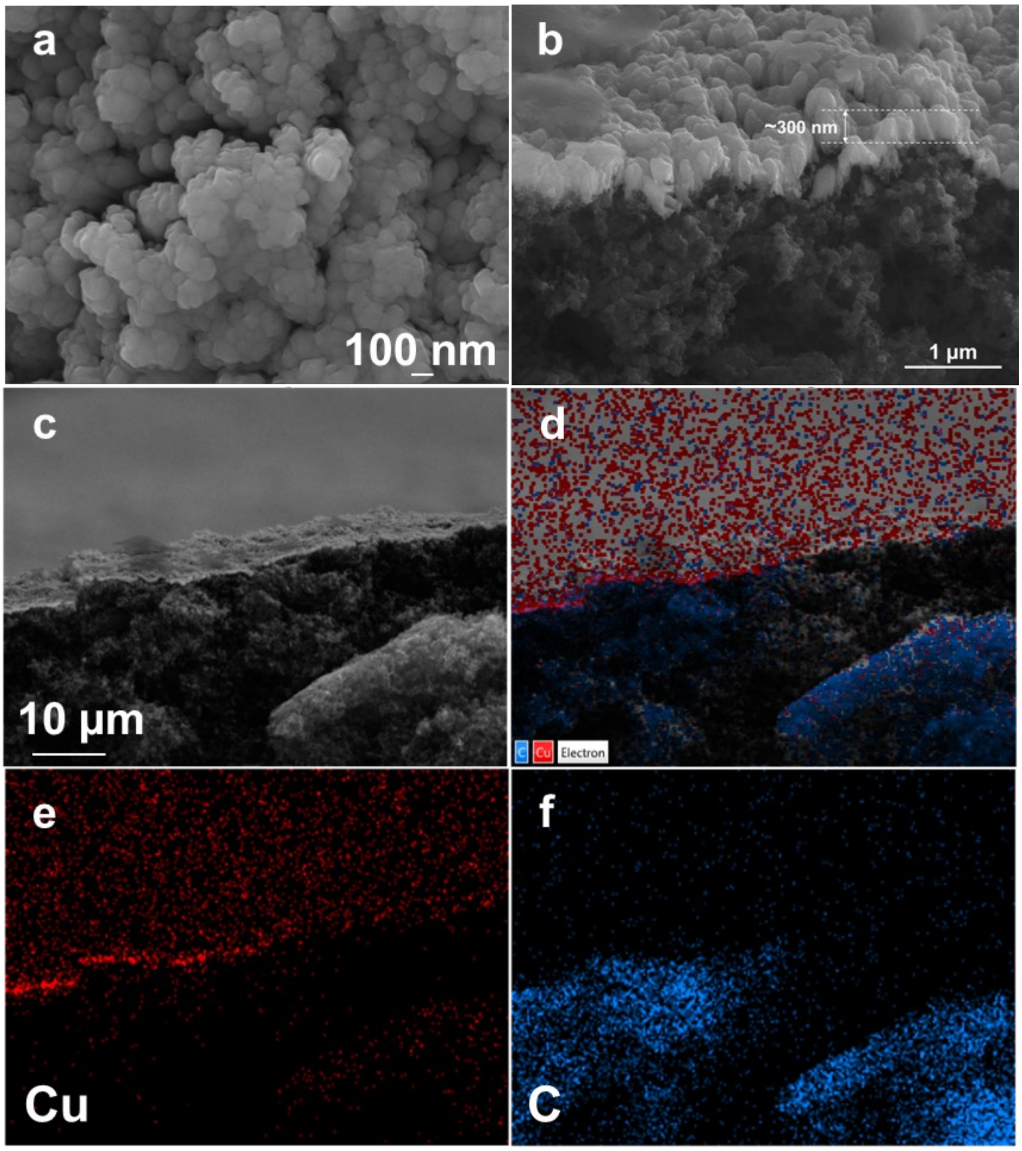

Figure S16. (a) SEM, (b, c) cross section SEM images and the (d-e) elemental mapping of the pristine Cu GDE.

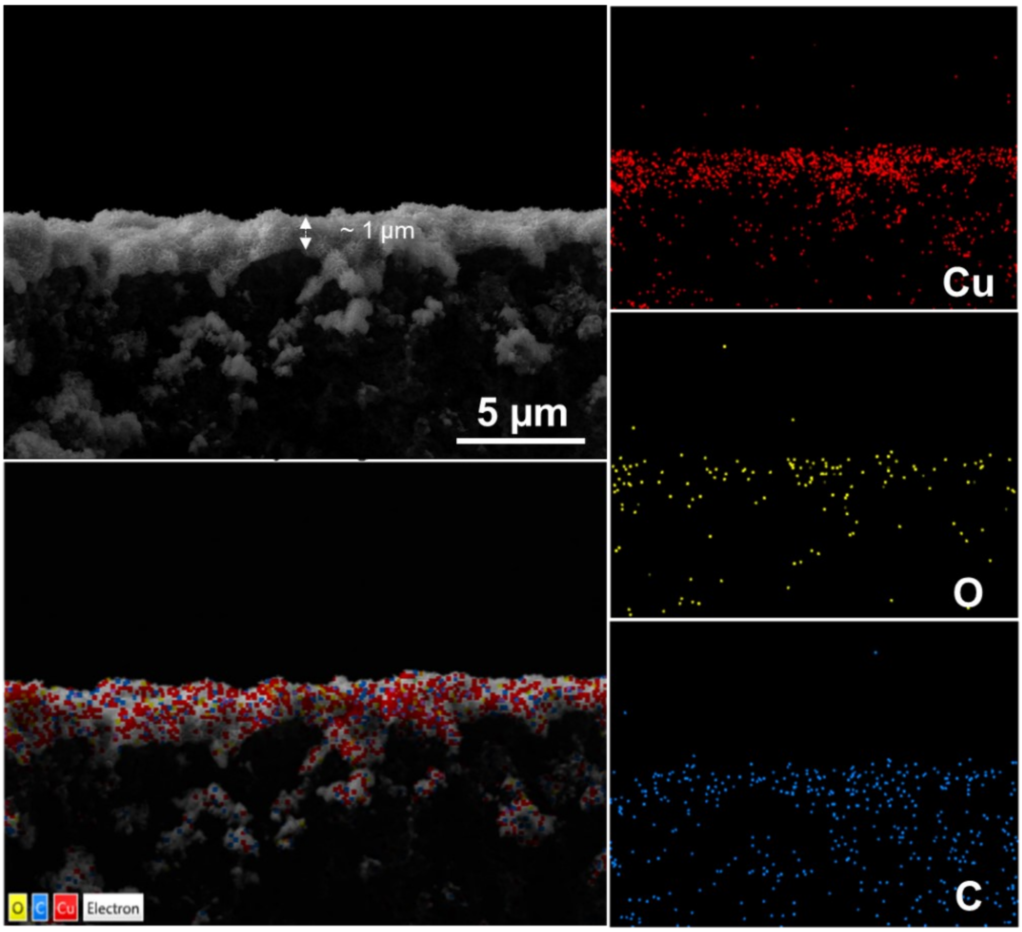

Figure S17. Cross section SEM image and the elemental mapping of the Cu NS GDE.

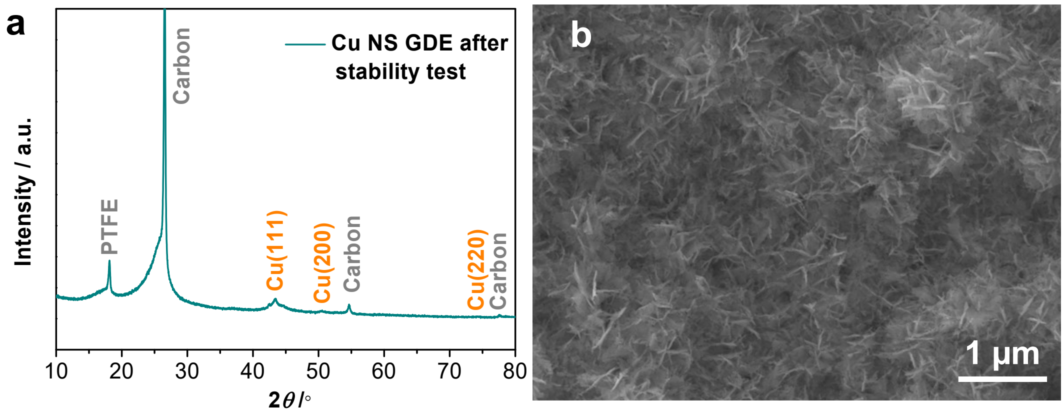

Figure S18. (a) XRD pattern and (b) SEM image of the Cu NS GDE electrode after stability test.

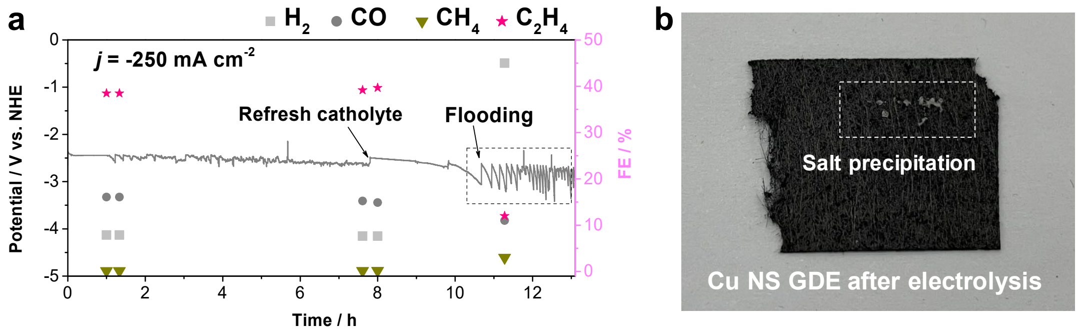

Figure S19. (a) Stability test of the Cu NS GDE at current density of -250 mA cm^{-2} for longer period in 1 M KOH. (b) The picture of the back side of Cu NS GDE after electrolysis. The salt precipitation was clearly marked in the white frame.

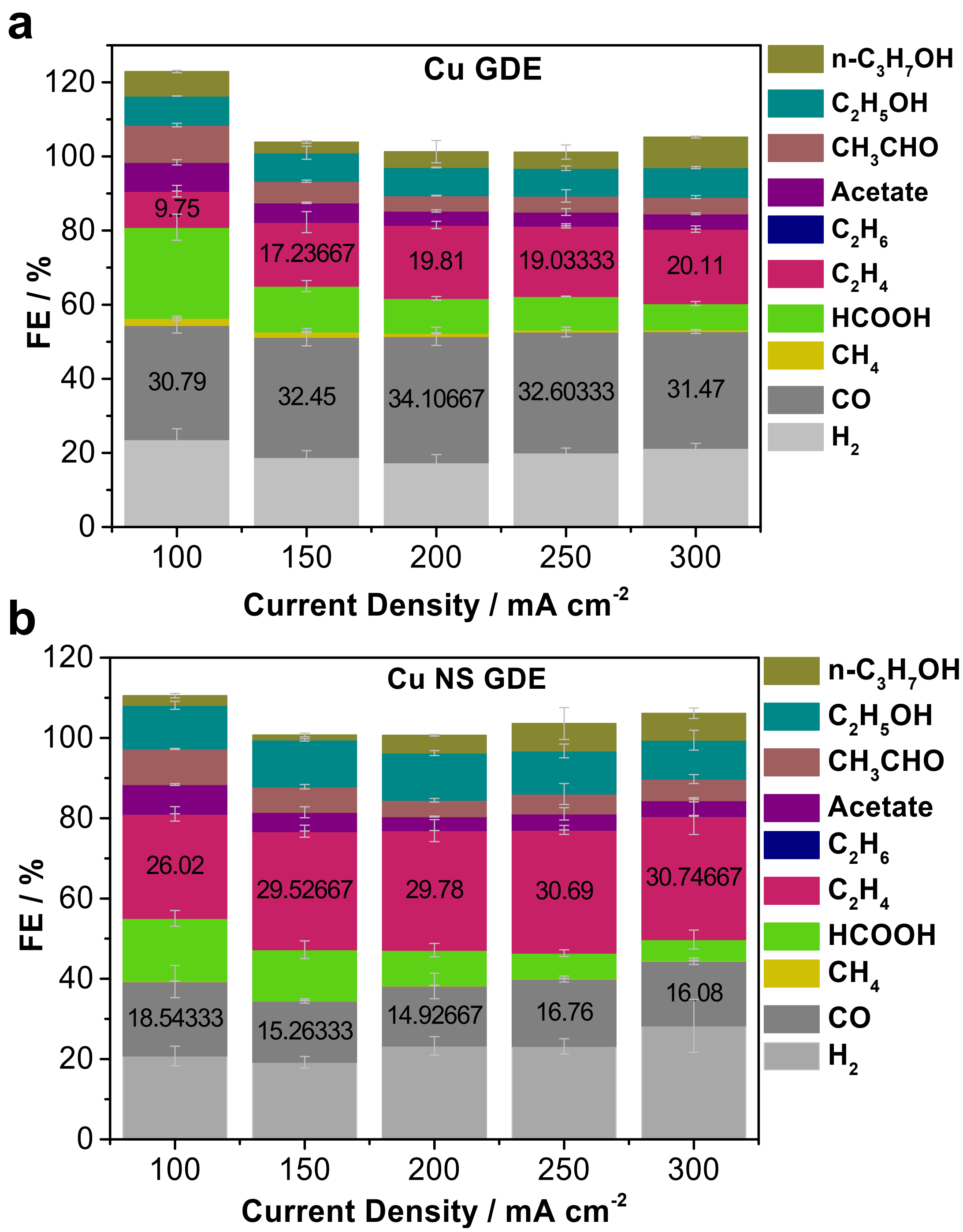

Figure S20. Faradaic efficiencies for all detectable products in 1 M $KHCO_3$ on (a) Cu and (b) Cu NS GDE. The FE of gaseous products was carefully calculated based on the outlet gas flow rates.

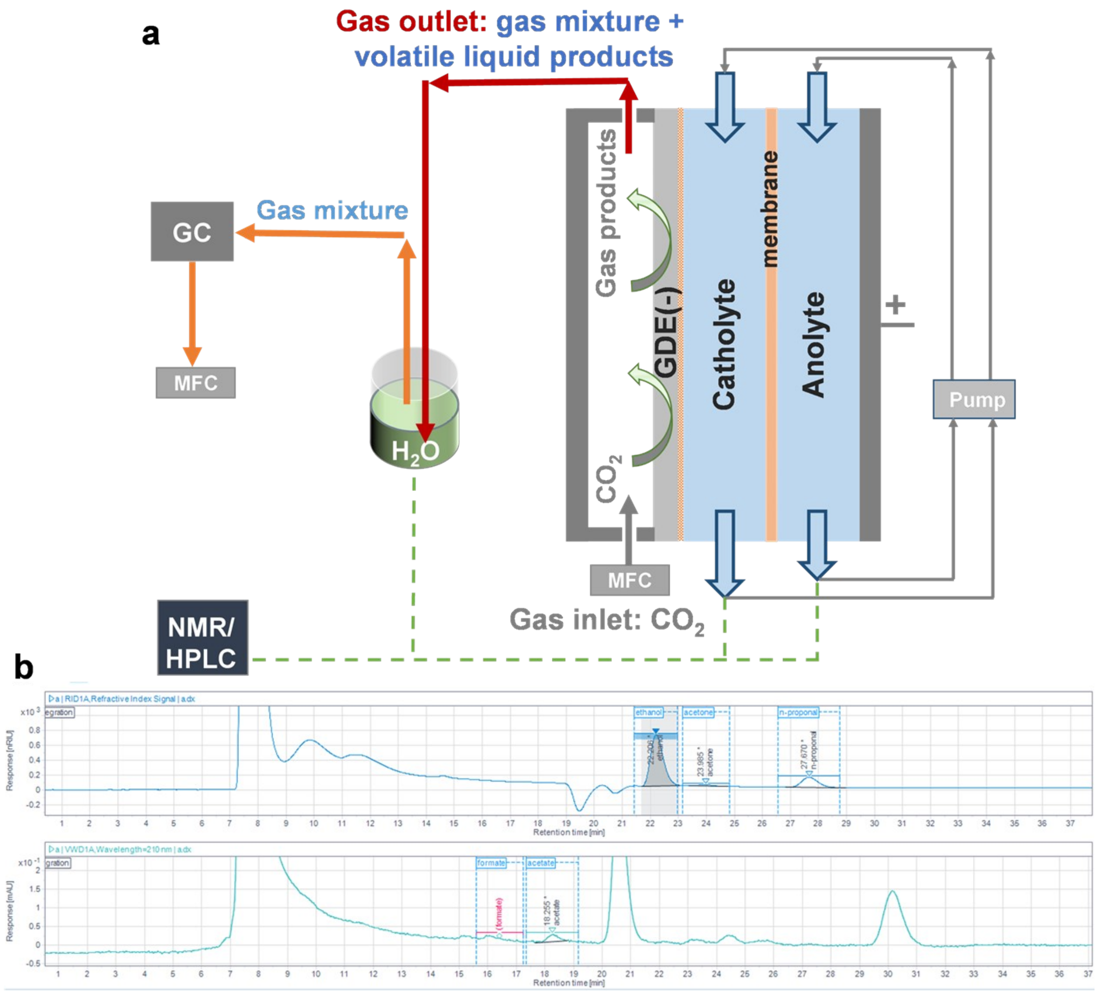

Figure S21. (a) schematic illustration of the modified flow cell system; (b) peaks of ethanol, acetone, n-propanol and acetate in the HPLC spectra for the trapped volatile liquid products by water from the outlet of the CO_2 component.

Table S1. Faradaic efficiency of all detectable products on Cu@Cu NS electrode for CO_2 RR at different applied potentials.

Potential V vs. RHE	H_2	CO	CH_4	HCOOH	C_2H_4	C_2H_6	Ethanol	Acetate	Acetone	n-Propanol
-1.246	27.89	2.38	2.83	10.55	36.20	0.22	12.60	0.33	4.27	4.99
-1.268	30.58	2.28	2.74	10.18	37.05	0.20	12.40	0.29	3.84	4.46
-1.296	27.25	2.25	3.37	8.55	36.35	0.20	14.75	0.31	3.86	4.93
-1.325	30.30	1.33	3.17	8.94	36.77	0.18	13.48	0.28	3.61	4.30
-1.357	27.03	1.82	3.62	6.44	40.70	0.18	14.69	0.32	3.38	4.64
-1.414	29.21	1.98	3.15	6.73	36.47	0.17	12.49	0.30	3.58	4.60
-1.458	29.42	2.2	3.32	6.60	35.71	0.19	14.30	0.29	3.16	4.90

Table S2. Faradaic efficiency of all detectable products on different Cu@Cu NS-x electrodes for CO_2 RR at -1.357 V *vs*. RHE.

Electrodes	H_2	CO	CH_4	HCOOH	C_2H_4	C_2H_6	Ethanol	Acetate	Acetone	n-Propanol
Cu@Cu NS-0	26.81	1.44	39.98	6.04	14.19	0.01	0.62	4.03	1.20	1.43
Cu@Cu NS-1	40.10	1.10	16.78	5.46	18.08	0.01	16.89	0.36	0.96	1.07
Cu@Cu NS-3	37.48	1.18	8.76	5.87	22.51	0.03	18.93	0.26	1.18	1.55
Cu@Cu NS-6	36.58	1.30	6.45	6.42	25.61	0.05	18.39	0.24	1.17	2.08
Cu@Cu NS-9	34.43	1.40	4.25	7.24	26.51	0.10	22.91	0.41	0.74	2.44
Cu@Cu NS-12	27.03	1.82	3.62	6.44	40.70	0.18	14.69	0.32	3.38	4.64
Cu@Cu NS-24	42.84	1.22	2.78	13.19	18.33	0.07	18.36	0.12	1.91	2.36
Cu@Cu NS-36	50.72	1.09	0.84	6.74	22.75	0.32	18.89	0.24	1.52	2.68

Table S3. Faradaic efficiency of all detectable products on Cu GDE for ECO_2 RR under different current density in 1 M KOH.

Current density /mA cm^{-2}	H_2	CO	CH_4	HCOOH	C_2H_4	CH_3CHO	Ethanol	Acetate	Acetone	n-Propanol
100	6.44	34.20	0.32	4.80	25.20	23.38	3.75	0.74	1.91	4.28
150	5.91	30.04	0.51	3.55	28.99	14.60	4.91	0.84	1.73	3.79
200	5.23	24.71	0.36	3.18	28.46	14.50	6.86	1.01	1.33	4.08
250	6.08	25.23	0.33	2.71	31.91	12.39	6.26	1.24	1.37	4.20
300	5.61	22.48	0.27	2.26	33.22	11.52	11.13	1.05	1.05	4.66
350	6.50	21.64	0.22	1.90	33.53	10.10	7.81	1.43	2.14	3.93
400	6.78	19.69	0.35	1.40	32.72	7.71	9.07	1.56	0.76	3.10

Table S4. Faradaic efficiency of all detectable products on Cu@Cu NS GDE for ECO_2 RR under different current density in 1 M KOH.

Current density /mA cm^{-2}	H_2	CO	CH_4	HCOOH	C_2H_4	CH_3CHO	Ethanol	Acetate	Acetone	n-Propanol
100	8.04	25.85	0.03	6.53	30.68	35.72	5.76	0.64	1.74	6.50
150	7.33	21.29	0.03	4.56	33.91	24.32	5.38	0.56	1.57	6.00
200	6.65	18.30	0.04	3.51	35.50	18.93	8.14	0.63	1.31	5.62
250	7.02	17.71	0.05	2.69	40.21	15.75	7.61	0.62	1.05	4.72
300	6.63	15.70	0.04	2.40	37.67	13.88	11.71	1.19	0.76	5.02
350	6.97	14.19	0.03	1.81	38.44	13.04	11.43	0.68	0.76	4.71
400	8.02	13.81	0.06	1.57	34.97	10.27	10.10	0.91	0.69	3.75

Table S5. Faradaic efficiency of all detectable products on Cu GDE for CO_2 RR under different current density in 1 M $KHCO_3$.

Current density /mA cm^{-2}	H_2	CO	CH_4	HCOOH	C_2H_4	CH_3CHO	Ethanol	Acetate	n-Propanol
100	23.59	30.79	1.98	24.54	9.75	10.06	7.84	7.76	6.61
150	18.79	32.45	1.40	12.38	17.24	5.86	7.67	5.21	2.88
200	17.36	34.11	0.81	9.43	19.81	4.16	7.61	3.75	4.26
250	20.04	32.60	0.56	9.04	19.03	4.35	7.48	3.73	4.36
300	21.28	31.47	0.48	7.07	20.11	4.51	7.97	4.11	8.22

Table S6. Faradaic efficiency of all detectable products on Cu@Cu NS GDE for CO_2 RR under different current density in 1 M $KHCO_3$.

Current density /mA cm^{-2}	H_2	CO	CH_4	HCOOH	C_2H_4	CH_3CHO	Ethanol	Acetate	n-Propanol
100	20.77	18.54	0.11	15.62	26.02	8.86	10.87	7.31	2.42
150	19.21	15.26	0.09	12.68	29.53	6.38	11.68	4.69	1.22
200	23.29	14.93	0.13	8.79	29.78	4.09	11.75	3.48	4.43
250	23.18	16.76	0.12	6.34	30.69	4.95	10.73	3.99	6.84
300	28.30	16.08	0.16	5.23	30.75	5.36	9.69	3.81	6.70

Table S7 Faradaic efficiency of all detectable products on Cu GDE for ECO RR under different current density in 1 M KOH.

Current density /mA cm^{-2}	H_2	CH_4	C_2H_4	C_2H_6	CH_3CHO	Ethanol	Acetate	n-Propanol
100	8.18	2.43	39.22	0.09	0.62	20.23	2.85	13.76
150	10.16	1.25	42.00	0.03	0.35	20.73	1.32	7.30
200	11.51	1.01	40.64	0.03	0.27	19.90	1.14	5.76
250	19.21	0.96	34.75	0.02	0.23	18.08	0.76	3.87
300	31.51	1.10	25.28	0.02	0.16	13.86	0.74	2.36

Table S8 Faradaic efficiency of all detectable products on Cu GDE for ECO RR under 200 mA cm^{-2} in 1 M KOH.

Current density /mA cm^{-2}	**H_2**	**CH_4**	**C_2H_4**	**C_2H_6**	**CH_3CHO**	**Ethanol**	**Acetate**	**n-Propanol**
200	7.10	1.32	36.51	0.05	0.30	19.55	2.79	7.26

Table S9. Electrocatalytic performances for CO_2 to C_{2+} products and fabrication strategies over electrodes test in H-cell reported recently.

Electrodes	**Fabrication strategies**	**Electrode area**	**Electrolyte**	***j*** **($mAcm^{-2}$)**	**FE for C_{2+} (%)**	**Ref.**
100-cycle Cu	Metal ion cycling	1 cm^2	0.25 M $KHCO_3$	~40	60	2
1.7 μm Cu2O film	Electrodeposition	Ø=10 mm	0.1 M $KHCO_3$	~13	~48	3
Plasma-activated Cu	Plasma treatment	/	0.1 M $KHCO_3$	~12	60	4
CuO spray nanoparticle	electrospray pyrolysis	16 cm^2	0.1 M $KHCO_3$	~22	~65	5
Cu/PANI	drop-casting	/	0.1 M $KHCO_3$	34.7	78.4	6
$Cu@Cu_2(OH)_3NO_3$	molten salt decomposition	2 cm^2	0.1 M $KHCO_3$	80	41.8	7
Re-Cu-I	electrochemical redox reconstruction	0.5×2.5 cm^2	0.1 M $KHCO_3$	21	80	8
NS-D Cu	electrochemical treatment	/	0.1 M $KHCO_3$	~30	~60	9
$Cu(OH)_2$	Hydrothermal	3 × 4 cm^2	0.1 M $KHCO_3$	~10	~20	10
Cu-O_2 plasma	O_2 Plasma treatment	/	0.1 M $CsHCO_3$	~8.5	58.8	11
Cu@Cu NS	Chemical corrosion	32 × 28cm^2	0.1 M $KHCO_3$	105	63.93	**This work**

Table S10. Electrocatalytic performances for CO_2 to C_{2+} products and fabrication strategies over electrodes test in flow cell reported recently.

Electrodes	**Fabrication strategies**	**Electrode area**	**Electrolyte**	***j*** **($mAcm^{-2}$)**	**FE for C_{2+} (%)**	**Ref.**
Hydrophobic Cu	Electrodeposition	/	1 M KOH	300	64±1.4	12
$Cu(OH)_2$/CP	Chemical corrosion	2*5 cm^2	1 M KOH	250	87	13
GB-Cu	Electrodeposition	2.25 cm^2	1 M KOH	96.62	70	14
P-doped Cu	Electrodeposition+ thermal treatment	4 cm^2	1 M KOH	328	64	15
Cu	magnetron sputtering	/	1 M KOH	250	~70	16
CuAg wire	Electrodeposition	2*5 cm^2	1 M KOH	310.8	85.1	17
Cu-DAT wire	Electrodeposition	2*5 cm^2	1 M KOH	210	70.2	18
Cu-P1	Electrodeposition	/	10 M KOH	/	＞87	19
Abrupt Cu	magnetron sputtering	/	10 M KOH	275	＞88	20
Cu-12	magnetron sputtering+ Electrodeposition	/	1 M $KHCO_3$	~250	83.5	21
Cu@Cu NS	Chemical corrosion	153 cm^2	1 M KOH	250	70	**This work**

Reference

1. L. Wan, X. Zhang, J. Cheng, R. Chen, L. Wu, J. Shi, and J. Luo, *ACS Catal*. **2022**, 12, 2741-2748.

2. K. Jiang, R. B. Sandberg, A. J. Akey, X. Liu, D. C. Bell, J. K. Nørskov, K. Chan and H. wang, *Nat. Catal.* **2018,** *1*, 111-119.

3. D. Ren, Y. Deng, A. D. Handoko, C. S. Chen, S. Malkhandi and B. S. Yeo, *ACS Catal.* ***2015,*** 5, 2814-2821.

4. H. Mistry, A. S. Varela, C. S. Bonifacio, I. Zegkinoglou, I. Sinev, Y-W Choi, K. Kisslinger, E. A. Stach, J. C. Yang, P. Strasser and B. R. Cuenya, *Nat. Commun.* ***2016***, 7, 12123-12131.

5. S. Y. Lee, S. Y. Chae, H. Jung, C. W. Lee, D. L. T. Nguyen, H.-S Oh, B. K. Min and Y. J. Hwang, *J. Mater. Chem. A,* ***2020***, 8, 6210-6218.

6. X. Wei, Z. Yin, K. Lyu, Z. Li, J. Gong, G. Wang, L. Xiao, J. Lu and L. Zhuang, *ACS Catal.* ***2020***, 10, 4103-4111.

7. M. Wang, Q. Z., Q. Xie, L. Wan, Y. Zhao, X. Zhanga and J. Luo, *Nanoscale* ***2020***, 12, 17013-17019.

8. J. Han, C. Long, J. Zhang, K. Hou, Y. Yuan, D. Wang, X. Zhang, X. Qiu, Y. Zhu, Y. Zhang, Z. Yang, S. Yan and Z. Tang, *Chem. Sci.* ***2020,*** 11, 10698-10704.

9. Y. Fu, Q. Xie, L. Wu, J. Luo, Chinese Journal of Catalysis, 2022, 43, 1066-1073.

10. Q. Xie, G. O. Larrazábal, M. Ma, I. Chorkendorff, B. Seger and J. Luo, *Journal of Energy Chemistry*, *63*, 278-284.

11. K. Jiang, Y. Huang, G. Zeng, F. M. Toma, W. A. Goddard, III and A. T. Bell, *ACS Energy Lett.* ***2020,*** 5, 1206-1214.

12. Z-Z Niu, F-Y Gao, X-L Zhang, P-P Yang, R Liu, L-P Chi, Z-Z Wu, S. Qin, X. Yu and M-R. Gao, *J. Am. Chem. Soc.* ***2021***, 143, 21, 8011-8021.

13. D. Zhong, Z-J Zhao, Q. Zhao, D. Cheng, B. Liu, G. Zhang, W. Deng, H. Dong, L. Zhang, J. Li, J. Li and J. Gong, *Angew. Chem. Int. Ed.* ***2021***, 60,4879-4885.

14. Z. Chen, T. Wang, B. Liu, D. Cheng, C. Hu, G. Zhang, W. Zhu, H. Wang, Z-J Zhao and J. Gong, *J. Am. Chem. Soc.* ***2020***, 142, 6878-6883.

15. X. Kong, C. Wang, H. Zheng, Z. Geng, J. Bao and J. Zeng, *Science China Chemistry,* ***2021***, 64, 1096-1102.

16. M. Ma, E. L. Clark, K. T. Therkildsen, S. Dalsgaard, I. Chorkendorff and B. Seger, *Energy Environ. Sci.,* ***2020***, 13, 977.

17. T. T. H. Hoang, S. Verma, S. Ma, T. T. Fister, J. Timoshenko, A. I. Frenkel, P. J. A. Kenis and A. A. Gewirth, *J. Am. Chem. Soc.* ***2018,*** 140, 17, 5791-5797.

18. T. T. H. Hoang, S. Ma, J. I. Gold, P. J. A. Kenis and A. A. Gewirth, *ACS Catal.* ***2017***, 7, 3313-3321.

19. X. Chen, J. Chen, N. M. Alghoraibi, D. A. Henckel1, R. Zhang, U. O. Nwabara, K. E. Madsen, P. J. A. Kenis, S. C. Zimmerman and A. A. Gewirth, *Nat Catal.* ***2021***, 4, 20-27.

20. C-T Dinh, T. Burdyny, M. G. Kibria, A. Seifitokaldani, C. M. Gabardo, F. P. G. de Arquer, Amirreza Kiani, J. P. Edwards, P. D. Luna, O. S. Bushuyev, C. Zou, R. Q-Bermudez, Y. Pang, D. Sinton and E. H. Sargent, *Science,* ***2018,*** 360, 783-787.

21. F. Li, A. T., A. R-Hernandez, Z. Wang, Y. Li, C. M. Gabardo, A. Ozden, C. T. Dinh, J. Li, Y. Wang, J. P. Edwards, Y. Xu, C. McCallum, L. Tao, Z. Liang, M. Luo, X. Wang, H. Li,

C. P. O'Brien, C-S Tan, D-H Nam, R. Q-Bermudez, T-T Zhuang, Y. C. Li, Z. Han, R. D. Britt, D. Sinton, T. Agapie, J. C. Peters and E. H. Sargent, *Nature* ***2020***, 577, 509-513.